

# A Parcellation Scheme for Human Left Lateral Parietal Cortex

Steven M. Nelson,<sup>1,\*</sup> Alexander L. Cohen,<sup>1</sup> Jonathan D. Power,<sup>1</sup> Gagan S. Wig,<sup>1</sup> Francis M. Miezin,<sup>1,2</sup> Mark E. Wheeler,<sup>7,8</sup> Katerina Velanova,<sup>8,9</sup> David I. Donaldson,<sup>6</sup> Jeffrey S. Phillips,<sup>7,8</sup> Bradley L. Schlaggar,<sup>1,2,3,4</sup> and Steven E. Petersen<sup>1,2,3,5</sup>

<sup>1</sup>Department of Neurology

<sup>2</sup>Department of Radiology

<sup>3</sup>Department of Anatomy and Neurobiology

<sup>4</sup>Department of Pediatrics

<sup>5</sup>Department of Psychology

Washington University, St. Louis, MO 63110, USA

<sup>6</sup>Department of Psychology, University of Stirling, Stirling FK9 4LA, UK

<sup>7</sup>Department of Psychology, Learning Research and Development Center

<sup>8</sup>Center for the Neural Basis of Cognition

<sup>9</sup>Department of Psychiatry

University of Pittsburgh, Pittsburgh, PA 15260, USA

\*Correspondence: [stevenelson@wustl.edu](mailto:stevenelson@wustl.edu)

DOI 10.1016/j.neuron.2010.05.025

## SUMMARY

The parietal lobe has long been viewed as a collection of architectonic and functional subdivisions. Though much parietal research has focused on mechanisms of visuospatial attention and control-related processes, more recent functional neuroimaging studies of memory retrieval have reported greater activity in left lateral parietal cortex (LLPC) when items are correctly identified as previously studied (“old”) versus unstudied (“new”). These studies have suggested functional divisions within LLPC that may provide distinct contributions toward recognition memory judgments. Here, we define regions within LLPC by developing a parcellation scheme that integrates data from resting-state functional connectivity MRI and functional MRI. This combined approach results in a 6-fold parcellation of LLPC based on the presence (or absence) of memory-retrieval-related activity, dissociations in the profile of task-evoked time courses, and membership in large-scale brain networks. This parcellation should serve as a roadmap for future investigations aimed at understanding LLPC function.

## INTRODUCTION

In humans, parietal cortex has traditionally been linked to processing mechanisms involving attention (Corbetta et al., 1998; Corbetta and Shulman, 2002; Dosenbach et al., 2006, 2007; Rushworth et al., 2001; Yantis et al., 2002). Other accounts of parietal cortex function, particularly focused on the left hemisphere, have examined its role in reading (Turkeltaub et al.,

2002), as well as numerosity judgments and arithmetic (Göbel and Rushworth, 2004; Hubbard et al., 2005). More recently, there has been a surge in research devoted to understanding the contributions of left lateral parietal cortex (LLPC) to memory retrieval (for review, see Wagner et al., 2005). The multitude of processing descriptions arising from studies in these domains suggests that distinct regions in parietal cortex might subservise unique functional contributions. As Devlin and Poldrack (2007) have argued, the success of functional neuroimaging is contingent on the ability to accurately and precisely map function to underlying neuroanatomy. The primary goal of the current study is to better define divisions that exist within LLPC. As a means of identifying potential distinctions, we use a combined resting-state functional connectivity MRI (rs-fcMRI) and functional MRI (fMRI) approach. The fMRI data includes studies related to memory retrieval, which will be used to leverage the distinctions seen with rs-fcMRI-based analyses and to better understand how specific LLPC regions contribute to this domain.

Determining the functional-neuroanatomical correlates of memory retrieval has driven a considerable amount of work in cognitive neuroscience. In particular, a great deal of research has been aimed at understanding how humans distinguish between previously experienced information (“old”) and that which is novel (“new”) (Henson et al., 2000; Konishi et al., 2000; McDermott et al., 2000; Wheeler and Buckner, 2003). Using fMRI, researchers have classified a set of regions in the brain that tend to be more active when human subjects correctly identify an item as old (“hit”) than when a given item is correctly identified as being new (“correct rejection”). This difference in activation has come to be called the “retrieval success effect” and is present in a highly distributed set of brain regions. The most common regions showing retrieval success effects are in lateral parietal cortex (Simons et al., 2008), and though this differential activation is typically bilateral, the most robust effects include a large expanse of LLPC (McDermott et al., 2009).

A number of laboratories (Cabeza et al., 2008; Ciaramelli et al., 2008; Vilberg and Rugg, 2008) have begun exploring the role of LLPC contributions to memory retrieval by performing metaanalyses in which data from large numbers of studies involving a variety of different retrieval tasks are analyzed in a common stereotactic space. The anatomical location of foci within LLPC can be differentiated on the basis of responses in paradigms contrasting recollection and familiarity, or source and item memory, as well as a number of other tasks in which old and new information is embedded. A consistent finding across these studies is the presence of a dorsal-ventral distinction in LLPC that appears to dissociate regions near intraparietal sulcus (IPS) involved in familiarity judgments (dorsal), and regions near angular gyrus involved in recollection (ventral) (Henson et al., 1999; Wheeler and Buckner, 2004).

Mapping estimates of recollection and familiarity onto distinct regions of LLPC represents one way in which the functional neuroanatomy underlying separate types of processing can be distinguished. However, even within the domain of memory retrieval, this distinction does not represent an extensive view of possible parcellations of LLPC. Further, a failure to incorporate “nonretrieval” related accounts of parietal mechanisms could result in an incomplete description of boundaries that exist within LLPC. A deeper understanding of the processing roles of LLPC is likely to be bolstered by the ability to apply objective parcellation schemes using a variety of analysis techniques.

One such technique, rs-fcMRI boundary mapping, is based on the observation that rs-fcMRI can dissociate regions within the cortex using edge-detection algorithms (Cohen et al., 2008). This procedure uses a seed-based approach (Biswal et al., 1995; Fox et al., 2005) to identify regions whose rs-fcMRI-derived time course is significantly correlated with the time course of the seed location. The result is a whole-brain correlation map that indicates the degree of correlation between the seed and all other voxels in the brain. Specifically, the technique developed in Cohen et al. (2008) detects transitions between whole-brain correlation maps of nearby cortical seeds, and translates these abrupt transitions into boundaries between cortical regions. A key concept underlying this approach that will be underscored by the present report is that *global brain relationships* can facilitate the parcellation of anatomically adjacent pieces of cortex.

The current study begins with such rs-fcMRI boundary mapping to identify “correlationally” distinct regions in LLPC. These regions then serve as a launching point from which to probe a set of recognition memory fMRI studies for distinctions within LLPC. We find that LLPC regions divide along anatomical lines into an anterior group that does not display retrieval success effects, and a posterior group that does. These findings are augmented with large-scale network analysis of rs-fcMRI signal correlations between LLPC regions and regions located outside of LLPC using tools from graph theory. This analysis confirms the anterior/posterior distinction and divides the retrieval success regions into four groups embedded in distinct whole-brain rs-fcMRI networks. This final LLPC parcellation scheme is then corroborated by demonstrating that within the distinct whole-brain networks, the task-evoked signals shown by LLPC regions are shared by distinct sets of regions outside of LLPC.

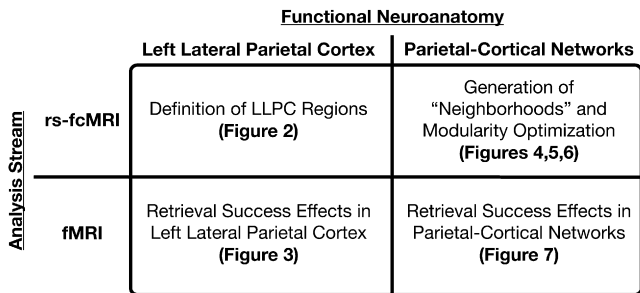


**Figure 1. An Outline of the Analysis Stream**

The analyses presented in the results comprise four sections represented in this 2 × 2 diagram.

## RESULTS

### Description of Analysis Stream

The results presented here can be viewed as the application of multiple analyses to two distinct imaging methodologies (fMRI and rs-fcMRI) both locally (within LLPC) and for distributed sets of regions (large-scale cortical networks) (Figure 1).

### Left Lateral Parietal Cortex: rs-fcMRI

#### **Fifteen Regions of Interest Were Defined within a Grid Applied to LLPC**

In order to parcellate LLPC and investigate its functional properties, an understanding of the local topography and heterogeneity is a critical starting point. The discovery that boundaries can be defined on the basis of abrupt changes in whole-brain rs-fcMRI maps (Cohen et al., 2008) provided a method (rs-fcMRI boundary mapping) by which to place regions of interest (ROI) in locations where rs-fcMRI maps are relatively stable and interrogate their function.

For the purposes of this experiment, a 27 × 27 grid of small spherical foci (6 mm diameter) was generated over the extent of LLPC (Figure 2A) using Caret software (Van Essen et al., 2001). The grid extended outside of traditional bounds of parietal cortex to decrease the chance that any functional borders near the anatomical boundaries of LLPC would go undetected.

The resulting rs-fcMRI boundary map that depicts the boundary likelihood at any given focus in the patch is shown in Figure 2B. “Hot” and “cool” colors indicate high and low probabilities, respectively, of the existence of a boundary.

The apparent centers of the bounded regions in LLPC were obtained by inverting the map such that “hot” colors now indicated rs-fcMRI map consistency between nearby seeds (Figures 2C and 2D). ROIs were defined as 10 mm diameter spheres at peak locations using 2D peak-finding algorithms. This resulted in 25 ROIs across the grid. Ten of the defined ROIs were outside of parietal cortex and were excluded from further analyses, leaving 15 LLPC ROIs as the targets of additional investigation.

### Left Lateral Parietal Cortex: fMRI

#### **Regions Located More Posteriorly in LLPC Showed Retrieval Success Effects**

We next applied these LLPC ROIs to a number of studies that contained a contrast of “old” versus “new” items and performed a

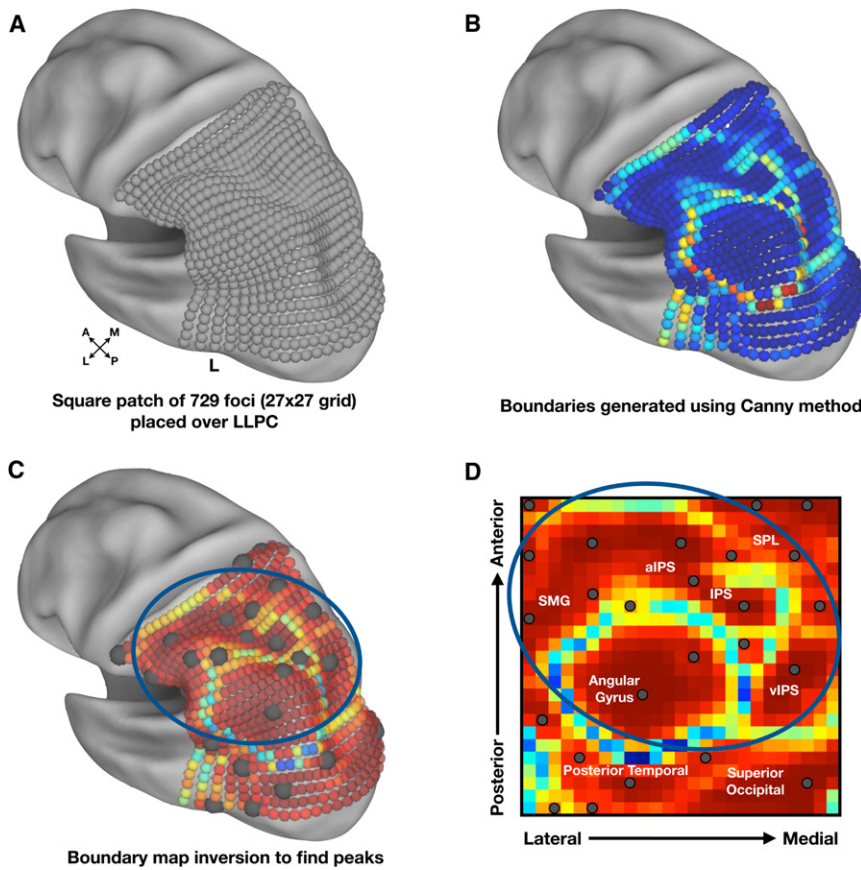


**Figure 2. rs-fcMRI Data Were Used to Generate Probabilistic Boundary Maps for the Purpose of Defining Regions in LLPC**

(A) A square patch of 729 spherical foci (6 mm diameter, 27 × 27 grid, spaced 6 mm apart) was created using Caret software (Van Essen et al., 2001) and is shown here on an inflated cortical surface rendering. The surface is rotated to allow better visualization of LLPC. A, anterior; P, posterior; L, lateral; M, medial.

(B) rs-fcMRI boundary map indicating the likelihood of a border at each seed. “Cooler” colors represent stable rs-fcMRI patterns, whereas “hotter” colors represent high border likelihood, i.e., rapidly changing rs-fcMRI patterns.

(C) Inverted rs-fcMRI boundary map demonstrating peaks of stability from the previous map. Centers are shown as dark gray spheres (10 mm diameter) on the inflated surface. The blue circle indicates regions of interest (ROI) located within LLPC.

(D) Unprojected data from (C) allowing better visualization of borders. Gray dots represent ROIs with those circled in blue indicating regions located within LLPC. For orientation purposes, the grid contains anatomical labels that roughly correspond to these locations on the cortical surface. SMG, supramarginal gyrus; SPL, superior parietal lobule; IPS, intraparietal sulcus.

metaanalysis (Table 1). Only the seven more posterior ROIs showed consistent retrieval success effects (Figure 3A, green circles), defining a strong functional boundary between region sets.

Previously, it was speculated that retrieval success regions may be divided through the examination of differential time course dynamics in adjacent regions and that this would be critical in determining an appropriate level of parcellation in LLPC (Wheeler and Buckner, 2004). With this in mind, we extracted time courses from three LLPC ROIs near those investigated in Wheeler and Buckner (2004) located in posterior middle intrapar-

ietal sulcus (pmIPS), posterior inferior parietal lobule (piPL), and angular gyrus (AG) (Figures 3B–3D) to determine whether there was a difference in their profiles. A region × time repeated-measures ANOVA with three levels of region and 14 levels of time (seven time points each for hit and cr) showed a significant interaction effect ( $F_{(12,84)} = 17.35, p < 0.001$ ). Post-hoc analyses revealed a significant region × time interaction for all three pairwise comparisons of time courses including pmIPS versus piPL ( $F_{(12,84)} = 13.13, p < 0.001$ ), pmIPS versus AG ( $F_{(12,84)} = 28.43, p < 0.001$ ), and piPL versus AG ( $F_{(12,84)} = 6.99, p < 0.001$ ).

**Table 1. Experimental Details for Tasks Included in the Analysis**

Study/Publication	Task Condition	Input Modality	Output Modality	Subjects
Donaldson et al. (2010)	source memory (target correct [hit] versus CR)	words	button	26
Phillips et al. (2009)	old/new (hit versus CR)	words	button	12
Velanova et al. (2003)	old/new (1 × hit versus 1 × CR) and old/new (20 × hit versus 20 × CR)	words	button	29
Wheeler and Buckner (2003)	source memory ([1 × hit + 20 × hit] versus CR)	pictures/sounds/words	button	29
Wheeler and Buckner (2004)	(remember [hit] + know [hit]) versus CR	pictures/words	button	20
Unpublished data <sup>a</sup>	old/new (hit versus CR) and old/new (hit versus CR)	words	button	24

Additional details can be found in the published manuscripts listed in the table.

<sup>a</sup> Unpublished data from two tasks wherein subjects are asked to respond “old” or “new” to words that they had either seen once or had not seen at all (standard old/new paradigm).

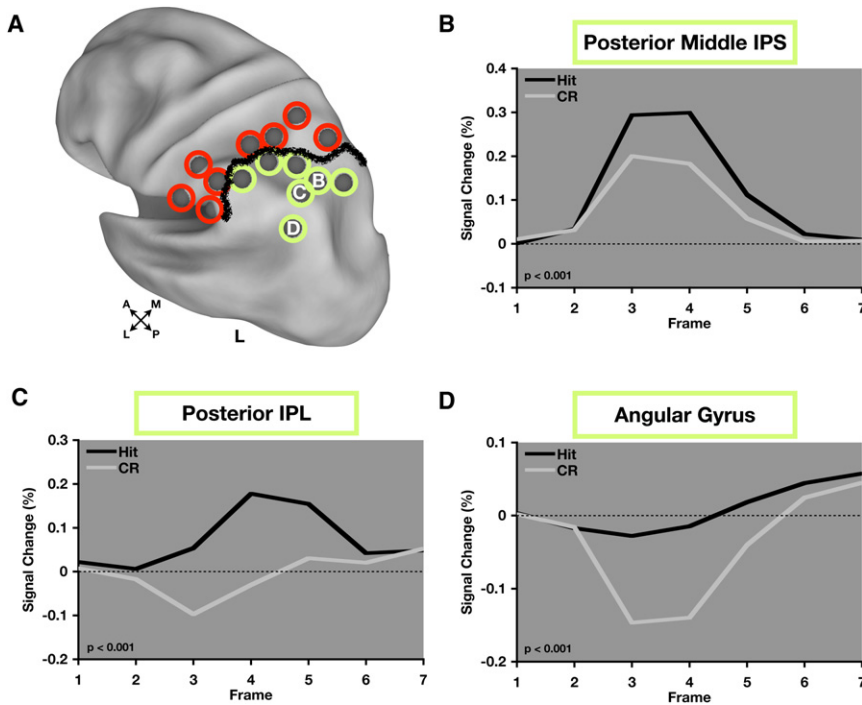


**Figure 3. Regions Showing Retrieval Success Effects Are Located in Posterior Parietal Cortex**

(A) ROIs circled in green indicate those that showed retrieval success effects across the eight studies that comprised the metaanalysis, while ROIs circled in red did not. The thick black line indicates this distinction. ROIs are displayed on inflated cortical surface renderings of the human brain using Caret software.

(B–D) Time courses from regions showing retrieval success effects. Posterior middle IPS (pmIPS), posterior IPL (pIPL), and angular gyrus (AG) time courses correspond to (B), (C), and (D) as labeled in (A). p values indicate level of significance for hit > correct rejection.

**Parietal-Cortical Networks: rs-fcMRI**

Since the initial definition of the LLPC regions was driven by differences in whole-brain rs-fcMRI relationships, one avenue toward addressing this ambiguity is to interrogate the whole-brain relationships of specific regions of LLPC. In other words, which regions outside of LLPC are

Although there is a clear statistical dissociation between IPS and AG time courses (Figures 3B and 3D), the time course in pIPL (Figure 3C) does resemble an average of IPS and AG time courses. Thus, while the time course in pIPL may reflect a truly distinct signal, the possibility exists that this is simply an artifact of the spatial averaging of the signals from pmIPS and AG. The close proximity of these regions poses problems as we attempt to draw functional distinctions. The question of how to resolve this ambiguity motivated, in part, the remaining analyses (Table 2).

most strongly functionally connected to each of the LLPC regions (the region’s “neighborhood”), and do regions in different neighborhoods show distinct functional time courses? If an LLPC region, such as pIPL, possesses a functional (fMRI), task-evoked time course reflecting some functional process, do other regions in its neighborhood share similar functional time courses? The following sections aim to provide answers to these questions through the exploration of relationships of LLPC regions to regions elsewhere in the brain. The next step

**Table 2. Response × Time Repeated-Measures ANOVA Performed on 15 LLPC ROIs**

LLPC Region	X	Y	Z	F Statistic <sub>(6,42)</sub>	p Value	Effect
Posterior IPS	-24	-67	48	<b>4.18</b>	<b>0.002</b>	<b>Hit &gt; CR</b>
Posterior middle IPS	-32	-62	48	<b>9.22</b>	<b>&lt;0.001</b>	<b>Hit &gt; CR</b>
Anterior middle IPS	-35	-53	49	<b>12.93</b>	<b>&lt;0.001</b>	<b>Hit &gt; CR</b>
Anterior IPS	-39	-44	44	<b>4.86</b>	<b>0.001</b>	<b>Hit &gt; CR</b>
Anterior IPL	-54	-47	48	<b>3.09</b>	<b>0.01</b>	<b>Hit &gt; CR</b>
AG	-45	-67	36	<b>10.97</b>	<b>&lt;0.001</b>	<b>Hit &gt; CR</b>
Posterior IPL	-40	-62	48	<b>8.97</b>	<b>&lt;0.001</b>	<b>Hit &gt; CR</b>
SMG	-56	-42	31	1.49	0.21	none
Anterior SMG	-63	-29	26	1.11	0.37	none
Anterior IPL	-60	-40	44	1.35	0.26	none
Lateral anterior IPS	-55	-28	38	0.87	0.52	none
Anterior IPS	-40	-37	47	1.64	0.16	none
Dorsal anterior IPS	-36	-41	54	<b>2.98</b>	<b>0.02</b>	<b>CR &gt; Hit</b>
SPL	-29	-44	65	<b>5.53</b>	<b>&lt;0.001</b>	<b>CR &gt; Hit</b>
Dorsal SPL	-24	-58	62	0.29	0.94	none

Significant statistical effects (p < 0.05) are shown in bold text. X, Y, and Z values correspond to stereotactic coordinates in MNI space.

is to define sets of regions that are related to LLPC regions using rs-fcMRI data.

**“Neighborhood” Generation Identified Regions Outside of LLPC Related to the LLPC ROIs**

Although rs-fcMRI boundary mapping and subsequent peak-finding algorithms can separate adjacent cortex into distinct regions based on underlying differences in rs-fcMRI correlation maps, they do not reveal what the actual underlying differences are that drive these spatial distinctions. To explore these differences, we generated rs-fcMRI “neighborhoods,” defined as the sets of regions most highly correlated with each of the 15 LLPC ROIs.

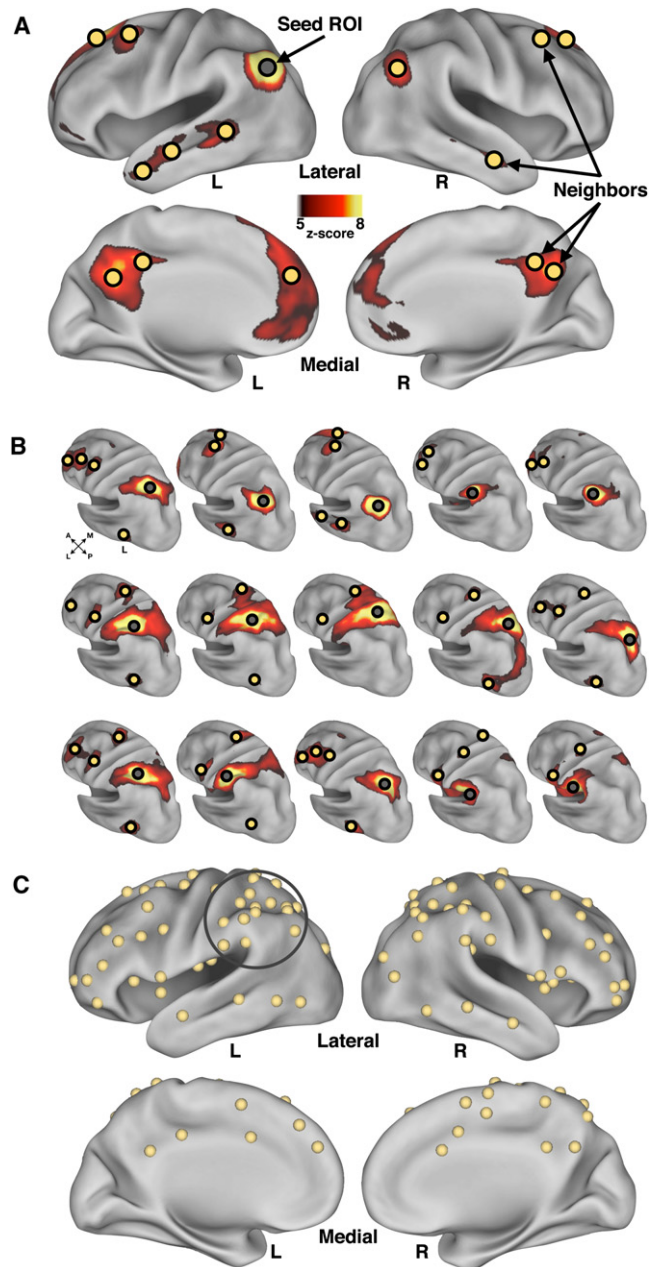
Figure 4A shows an example neighborhood derived from a seed location in left AG, one of the LLPC ROIs examined in the previous analysis (see Figure 3D). For a given seed location, the 15 most correlated regions were included to ensure a manageable aggregate set from all LLPC ROIs (see Experimental Procedures section on rs-fcMRI “Neighborhood” generation). It is important to note that since boundaries indicate abrupt change in whole-brain rs-fcMRI maps, adjacent regions will likely contain different, but potentially overlapping, sets of neighbors.

Figure 4B depicts the seed maps for all 15 LLPC ROIs and a portion of the identified neighbors for each ROI on the left lateral surface of the cortex. Neighbors that appeared in more than one seed map were consolidated to eliminate overlap (see Experimental Procedures), resulting in 87 final neighbors that spanned the cortex and cerebellum (Figure 4C, cerebellum not shown). The 87 neighbors and 15 LLPC ROIs formed a collection of 102 ROIs, which could then be viewed as a network of 102 nodes related to each other by rs-fcMRI correlations.

**Modularity Optimization Identified Four Modules within the 102 ROIs**

The next set of analyses was aimed at understanding this network, and in particular, whether distinct groupings or “modules” existed within the network, which might provide further distinctions between the LLPC ROIs. Tools from graph theory have become instrumental in determining structure within large-scale brain networks (Bullmore and Sporns, 2009; Sporns and Zwi, 2004). Networks are collections of items (nodes) possessing pairwise relations (edges) between each item, and community-detection analyses can decompose networks into functionally related subsets of nodes called “communities” or “modules.” For example, a person’s social network might include a module of coworkers, a module of relatives, and a module of teammates, each of which is richly connected internally, but possesses few connections to other modules. To assess the underlying grouping of our LLPC ROIs and their neighbors, community detection analysis using modularity optimization (Newman, 2006) was performed on the matrix of pairwise rs-fcMRI correlations between the 102 ROIs.

Modularity optimization separated the ROIs derived from the neighborhood analysis into four distinct sets of regions, or modules (Figure 5; Figure S1, available online). The supramarginal gyrus (SMG) module (blue, Figures 5A and 5B; Table 3) included regions in bilateral SMG, anterior and posterior insula,



**Figure 4. Generation of Neighborhoods for Each Location within LLPC Yielded 87 Additional Regions of Interest**

(A) An example neighborhood (yellow spheres) derived from a seed location (gray sphere) in left AG (one neighbor in right cerebellum not shown). (B) Left hemisphere view of each seed’s z-score normalized correlation map. Seed ROIs are indicated by a gray sphere and neighbors for each seed are indicated by yellow spheres. (C) Aggregate neighbor ROIs (102 total) from all 15 neighborhoods. Overlapping regions derived from multiple neighborhoods were combined by averaging in stereotactic space. Gray circle indicates the original 15 LLPC ROIs.

frontal operculum, dorsal anterior cingulate cortex (dACC), and supplementary motor area (SMA). The superior parietal lobule (SPL) module (orange, Figures 5A and 5B; Table 3) contained

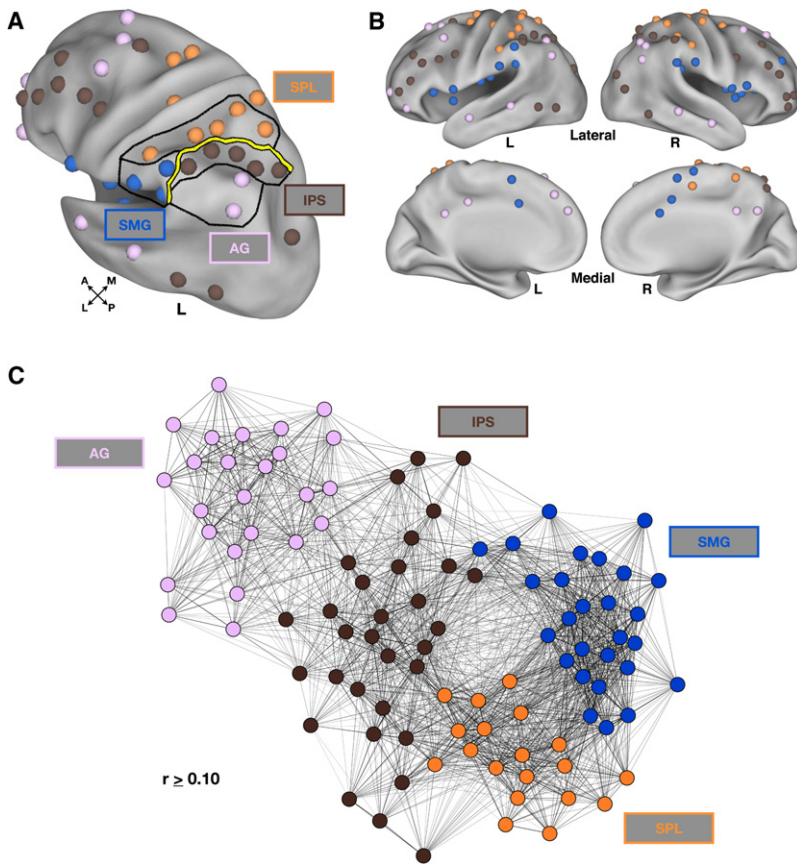


**Figure 5. Modularity Optimization Identified Four Modules within the Neighborhoods Generated from the 15 Seed Locations**

(A) Modularity optimization assignments shown in LLPC. Lines drawn in LLPC delineate the module assignments (SMG, blue; SPL, orange; IPS, brown; AG, light purple). The thick yellow line indicating the functional distinction made based on the presence or absence of retrieval success effects (Figure 3) was replicated using modularity optimization.

(B) Modularity optimization assignments shown on lateral and medial views using Caret software. Colors are same as in (A).

(C) Modularity optimization assignments are represented by the color of each of the nodes (colors are same as in A). The placement of each node is determined by a spring-embedding algorithm that takes into account both the presence and strength of node-node connections (rs-fcMRI correlations). The graph represents the global relaxation of the connections at a threshold ( $R \geq 0.10$ ) into a low energy state (see also Figure S1).

yellow line in Figure 5A, separating anterior from posterior modules/regions in an identical manner.

#### Hierarchical Structure in Modules Containing Retrieval Success Effects Revealed a Further Distinction in LLPC ROIs

We next conducted two modularity optimization analyses separately on retrieval success regions (the AG and IPS modules) and nonretrieval success regions (the SMG and SPL modules). This was done to determine whether there was further division among functionally similar regions that might have been overshadowed in a modularity optimization procedure containing functionally disparate regions.

Performing modularity optimization on the set of nonretrieval success regions did not result in any additional parietal distinctions from the SMG and SPL module assignments seen in the initial large-scale analysis. However, regions in SMA and dACC were placed into a small separate “submodule” (dark green, Figures 6A and 6D; Table 3; Figure S2, available online). Because the SMG module also contained regions along the extent of the bilateral insula, the final submodule will be referred to as the SMG/insula submodule (blue, Figures 6A, 6C, and 6D; Table 3). Additionally, because the final SPL submodule also contained regions in putative human FEF, it will be referred to as the SPL/FEF submodule (orange, Figures 6A, 6C, and 6D; Table 3).

Modularity optimization of the LLPC retrieval success regions (AG and IPS modules) revealed distinctions not seen in the large-scale modularity analysis. The original IPS module was separated into four distinct submodules, two of which contained original LLPC ROIs. One of these submodules (light blue, here labeled LIPS/dIPFC) contained four LLPC ROIs that lined the IPS, as well as other regions in frontal and temporal cortex (Figures 6B–6D; Table 3; Figure S2). The second submodule (light green, here labeled aIPL/aPFC) contained an LLPC region

regions in bilateral SPL, putative human “frontal eye fields” (FEF), anterior IPS, and postcentral gyrus. The IPS module (brown, Figures 5A and 5B; Table 4) included regions in bilateral IPS, dorsal frontal cortex, dorsolateral prefrontal cortex (dlPFC), anterior PFC (aPFC), and lateral temporal cortex. The AG module (light purple, Figures 5A and 5B; Table 4) consisted of regions in bilateral AG, posterior cingulate, medial PFC (mPFC), superior frontal gyrus (FG), ventrolateral PFC, anterior lateral temporal cortex, posterior IPL, and right cerebellum.

These assignments can be visualized using a spring-embedding algorithm in which the placement of each region or node in 2D space (Figure 5C) reflects relative node-node connection strengths. Thus, there should be visual overlap between relationships defined by modularity and spring embedding as both are dictated by correlations between the same set of regions, and this is the case here (Figure 5C).

The graph theory analyses revealed four modules, all of which contained regions both within LLPC and throughout the rest of the brain (Figures 5A and 5B). Strikingly, even though the modularity analysis contained no a priori information with regard to retrieval success effects, it still finds the same distinction within LLPC between regions in SPL and SMG and those located in AG and IPS. The dissociation found based on the presence or absence of a retrieval success effect across the LLPC ROIs (see Figure 3A) is replicated exactly and is extended in the modularity optimization analysis. This result is indicated by the thick

**Table 3. Regions Belonging to the SPL and SMG Modules and Their Corresponding Submodule Assignment**

Region	X	Y	Z	Module	Submodule
R lateral anterior IPS (1)	55	-20	42	SPL	SPL/FEF
R FEF (2)	26	-4	55	SPL	SPL/FEF
R SPL (3)	25	-51	64	SPL	SPL/FEF
R anterior IPS (4)	42	-33	51	SPL	SPL/FEF
L FEF (5)	-27	-7	55	SPL	SPL/FEF
R FEF (6)	25	-15	69	SPL	SPL/FEF
L FEF (7)	-18	-10	63	SPL	SPL/FEF
L SPL (8)	-17	-47	68	SPL	SPL/FEF
R SPL (9)	35	-37	62	SPL	SPL/FEF
R SPL (10)	14	-46	60	SPL	SPL/FEF
L anterior IPS (11)	-44	-25	56	SPL	SPL/FEF
R postcentral gyrus (12)	39	-17	60	SPL	SPL/FEF
R SPL (13)	18	-33	60	SPL	SPL/FEF
L medial anterior IPS (14)	-40	-37	47	SPL	SPL/FEF
L lateral anterior IPS (15)	-55	-28	38	SPL	SPL/FEF
L SPL (16)	-24	-58	62	SPL	SPL/FEF
L SPL (17)	-29	-44	65	SPL	SPL/FEF
L anterior IPS (18)	-36	-41	54	SPL	SPL/FEF
R SMA (19)	9	-11	52	SPL	SMA/dACC
L SMA (20)	-1	-1	52	SMG	SMA/dACC
L dorsal anterior cingulate (21)	-5	8	37	SMG	SMA/dACC
R SMA (22)	2	-6	64	SMG	SMA/dACC
R SMA (23)	8	3	59	SMG	SMA/dACC
R dorsal anterior cingulate (24)	1	16	28	SMG	SMA/dACC
R pre-SMA (25)	5	6	42	SMG	SMA/dACC
L anterior IPL (26)	-60	-40	44	SMG	SMG/insula
L inferior frontal (27)	-47	-1	13	SMG	SMG/insula
R inferior frontal (28)	39	-2	13	SMG	SMG/insula
R middle insula (29)	39	5	2	SMG	SMG/insula
R inferior frontal (30)	60	7	3	SMG	SMG/insula
L anterior insula (31)	-31	17	5	SMG	SMG/insula
R anterior insula (32)	36	20	7	SMG	SMG/insula
R SMG (33)	65	-24	25	SMG	SMG/insula
L middle insula (34)	-40	2	-1	SMG	SMG/insula
L inferior frontal (35)	-56	6	5	SMG	SMG/insula
R inferior frontal (36)	51	0	8	SMG	SMG/insula
R inferior frontal (37)	58	16	11	SMG	SMG/insula
R anterior PFC (38)	35	49	32	SMG	SMG/insula
R SMG (39)	68	-39	30	SMG	SMG/insula
L posterior insula (40)	-36	-16	-4	SMG	SMG/insula
L inferior frontal (41)	-56	-16	12	SMG	SMG/insula
L inferior frontal (42)	-51	-22	22	SMG	SMG/insula
R inferior frontal (43)	45	12	-4	SMG	SMG/insula
R SMG (44)	53	-34	26	SMG	SMG/insula
L SMG (45)	-56	-42	31	SMG	SMG/insula
L SMG (46)	-63	-29	26	SMG	SMG/insula

X, Y, and Z values correspond to stereotactic coordinates in MNI space. IPS, intraparietal sulcus; FEF, "frontal eye fields;" SPL, superior parietal lobule; SMA, supplementary motor area; SMG, supramarginal gyrus.

in left aIPL, along with a region in right aIPL, and regions in bilateral aPFC (Figures 6B–6D; Table 3). The "non-LLPC submodules" included a submodule that contained regions in right IPS and right dIPFC (purple, RIPS/dIPFC; Figures 6B and 6D; Table 3), while a fourth small submodule contained regions in superior occipital cortex (teal, Figures 6B and 6D; Table 3).

The original AG module was separated into three distinct submodules, two of which included original LLPC regions. An AG/mPFC submodule (red, Figures 6B–6D; Table 3) contained regions in medial frontal, temporal, and medial parietal cortex, while a pIPL/sFG submodule (light yellow, Figures 6B–6D; Table 3) included regions in superior frontal, anterior prefrontal, and lateral temporal cortex. A third submodule that was not highly interconnected with either the AG/mPFC or pIPL/sFG submodules consisted of three regions in right cerebellum (light brown, Figure 6B; Table 3).

Thus, as a result of modularity optimization on the AG and IPS modules, a total of four submodules emerged that included a region or regions within LLPC that exhibited retrieval success effects in the initial fMRI analysis. In total, six submodules were defined in LLPC. Importantly, the three LLPC regions that showed the apparently distinct time course profiles (see Figure 3) were also dissociated in the submodule analysis.

#### Parietal-Cortical Networks: fMRI

The final analysis seeks, in part, to further corroborate whether the previously described intermediate time course in pIPL (see Figure 3C) is functionally distinct by examining the time courses in regions within its submodule. If they show a similar pattern to the region in pIPL and are distinct from the AG/mPFC and LIPS/dIPFC submodules, this would indicate that the pIPL time course is indeed not an artifact of spatial blurring in LLPC. More generally, this analysis asks to what degree the distinctions found using rs-fMRI are reflected in task-evoked signals.

#### Regions Outside of LLPC Demonstrate Similar Retrieval Success Effects and Time Course Dynamics

The characterization of submodules that consist of regions outside of, but closely related to, each of the LLPC ROIs now provides an opportunity to assess task-evoked signals at the submodule level. Time courses for hits and correct rejections were extracted from the regions comprising each of the four submodules that contained an LLPC ROI exhibiting retrieval success effects (see Table 2) across the eight tasks that defined the initial metaanalysis. It is important to note that the following analyses were performed on submodule ROIs in which the original time courses from LLPC ROIs were excluded. As such, any observed effects are necessarily independent of the initial fMRI analysis that only examined LLPC ROIs.

We first conducted a submodule × time repeated-measures ANOVA with four levels of submodule and 14 levels of time (seven time points each for hit and cr) to determine whether the distinctions among the time course profiles in specific LLPC ROIs (Figures 7A–7D, and see Figure 3) were also present at the submodule level. The omnibus ANOVA yielded a significant effect of submodule × time ( $F_{(18,174)} = 13.27, p < 0.001$ ) and post-hoc tests were performed on all pairwise combinations of submodules (Table 5). This yielded significant effects of submodule

**Table 4. Regions Belonging to the AG and IPS Modules and Their Corresponding Submodule Assignment**

Region	X	Y	Z	Module	Submodule
L posterior cingulate (47)	-1	-31	39	AG	AG/mPFC
L anterior temporal (48)	-59	-7	-17	AG	AG/mPFC
R posterior cingulate (49)	1	-60	36	AG	AG/mPFC
R posterior cingulate (50)	3	-47	35	AG	AG/mPFC
R superior frontal (51)	19	35	50	AG	AG/mPFC
R angular gyrus (52)	50	-60	34	AG	AG/mPFC
L posterior cingulate (53)	-7	-54	31	AG	AG/mPFC
L dorsomedial PFC (54)	-3	50	24	AG	AG/mPFC
R anterior temporal (55)	63	-7	-17	AG	AG/mPFC
L angular gyrus (56)	-45	-67	36	AG	AG/mPFC
L superior frontal (57)	-18	29	54	AG	AG/mPFC
R lateral cerebellum (58)	35	-72	-32	AG	cerebellum
R medial cerebellum (59)	15	-84	-28	AG	cerebellum
R lateral cerebellum (60)	35	-65	-41	AG	cerebellum
L anterior PFC (61)	-32	57	1	AG	piPL/sFG
L middle temporal (62)	-63	-39	-4	AG	piPL/sFG
R middle temporal (63)	71	-37	-6	AG	piPL/sFG
R posterior IPL (64)	44	-56	41	AG	piPL/sFG
R superior frontal (65)	40	17	57	AG	piPL/sFG
R posterior IPL (66)	44	-63	52	AG	piPL/sFG
L dorsal anterior cingulate (67)	-10	40	41	AG	piPL/sFG
L superior frontal (68)	-31	17	55	AG	piPL/sFG
L superior frontal (69)	-44	12	46	AG	piPL/sFG
L posterior IPL (70)	-40	-62	48	AG	piPL/sFG
L ventrolateral PFC (71)	-45	47	-11	AG	aiPL/aPFC
L superior frontal (72)	-29	6	61	IPS	piPL/sFG
R anterior PFC (73)	38	30	42	IPS	aiPL/aPFC
L anterior IPL (74)	-54	-47	48	IPS	aiPL/aPFC
R anterior IPL (75)	56	-38	52	IPS	aiPL/aPFC
R anterior PFC (76)	43	61	2	IPS	aiPL/aPFC
R anterior PFC (77)	40	48	-2	IPS	aiPL/aPFC
R ventrolateral PFC (78)	47	52	-13	IPS	aiPL/aPFC
L anterior PFC (79)	-44	51	4	IPS	aiPL/aPFC
L dorsolateral PFC (80)	-38	35	30	IPS	LIPS/dIPFC
L dorsal frontal (81)	-47	3	32	IPS	LIPS/dIPFC
L posterior temporal (82)	-52	-58	-6	IPS	LIPS/dIPFC
L dorsolateral PFC (83)	-42	38	11	IPS	LIPS/dIPFC
L dorsolateral PFC (84)	-45	29	25	IPS	LIPS/dIPFC
L dorsal frontal (85)	-39	15	25	IPS	LIPS/dIPFC
L anterior middle IPS (86)	-35	-53	49	IPS	LIPS/dIPFC
L posterior IPS (87)	-24	-67	48	IPS	LIPS/dIPFC
L anterior IPS (88)	-39	-44	44	IPS	LIPS/dIPFC
L posterior middle IPS (89)	-32	-62	48	IPS	LIPS/dIPFC
R medial IPS (90)	18	-64	59	IPS	RIPS/dIPFC
R posterior temporal (91)	53	-56	-9	IPS	RIPS/dIPFC
R dorsolateral PFC (92)	47	42	19	IPS	RIPS/dIPFC
R dorsal frontal (93)	47	9	31	IPS	RIPS/dIPFC

**Table 4. Continued**

Region	X	Y	Z	Module	Submodule
R middle IPS (94)	41	-43	45	IPS	RIPS/dIPFC
R precuneus (95)	9	-69	54	IPS	RIPS/dIPFC
R posterior IPS (96)	28	-68	50	IPS	RIPS/dIPFC
R posterior middle IPS (97)	32	-51	48	IPS	RIPS/dIPFC
R dorsolateral PFC (98)	38	30	22	IPS	RIPS/dIPFC
L posterior temporal (99)	-48	-72	-2	IPS	RIPS/dIPFC
L superior occipital (100)	-26	-80	28	IPS	superior occipital
R superior occipital (101)	47	-77	13	IPS	superior occipital
R superior occipital (102)	38	-80	23	IPS	superior occipital

X, Y, and Z values correspond to stereotactic coordinates in MNI space. PFC, prefrontal cortex; IPL, inferior parietal lobule; IPS, intraparietal sulcus.

× time for five of the six comparisons, with the exception being piPL/sFG versus aiPL/aPFC (Table 5). Thus, the time course profiles between the AG/mPFC, piPL/sFG, and LIPS/dIPFC submodules are distinct from one another, mirroring both the apparent time course distinctions of Figure 3, and the modularity analysis that defined submodules (see Figure 6). Additionally, regions in the piPL/sFG and aiPL/aPFC submodules were dissociable throughout all levels of the rs-fcMRI analyses (see Figures 5 and 6); however, the lack of a submodule × time interaction suggests that each may contain a similar processing mechanism by virtue of their time course profiles.

We were also interested in determining which submodules, if any, showed retrieval success effects. Importantly, each of the four submodules showed a significant response × time interaction (two levels of response and seven levels of time) when averaging across regions outside of LLPC (Figures 7E–7H; Table 5), such that hits were greater than correct rejections. Additionally, we examined whether or not response × time interactions were present in submodules whose LLPC ROIs did not originally show retrieval success effects (SPL/FEF and SMG/insula). Neither submodule exhibited an effect of response × time (data not shown), which again mirrors the effects seen in the related LLPC regions.

## DISCUSSION

By applying graph theoretic tools and image analysis algorithms to a combination of functional and resting-state data, we were able to tease apart details of cortical network architecture. The result of these analyses was a parcellation scheme for LLPC that was informed by distinct types of data, the convergence of which lends credence to the LLPC boundaries and networks defined here. We think that this work provides a new lens by which to view LLPC and should inform functional studies by providing an anatomical platform from which to map information processing within this large region of cortex.

Generally speaking, the rs-fcMRI boundary mapping approach has the ability to provide unique insight into the structure

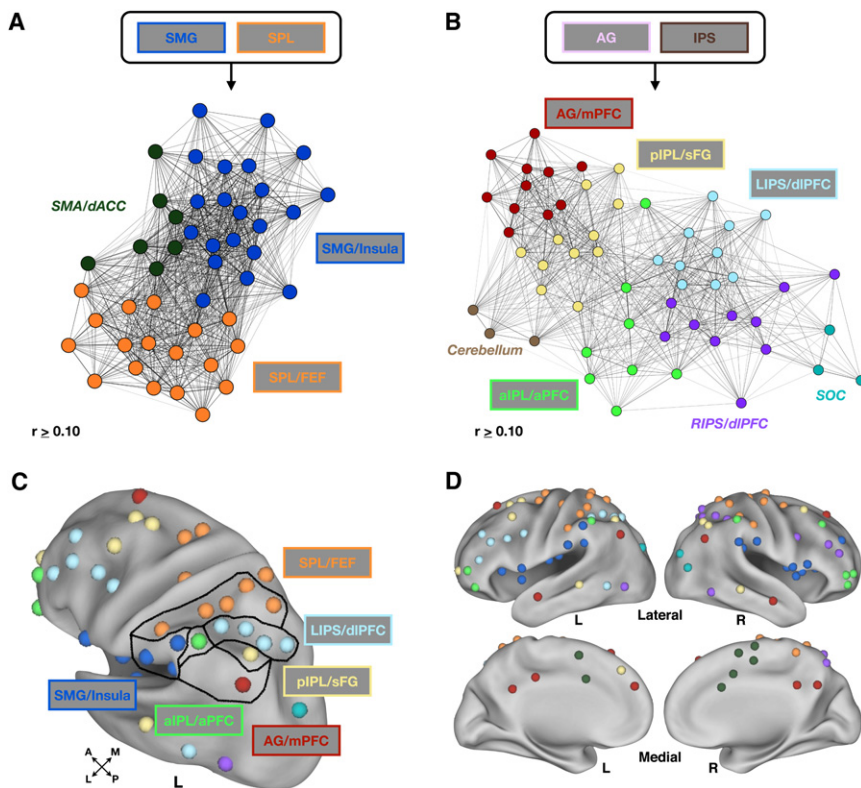


**Figure 6. Modularity Optimization Performed Separately on Modules Not Showing Retrieval Success Effects (SPL and SMG) and Retrieval Success Modules (AG and IPS)**

(A) The SPL and SMG modules did not split into separate submodules, though regions within the supplementary motor area (SMA) and dorsal anterior cingulate cortex (dACC) separate from the two (SMA/dACC, dark green). The SPL module is now labeled SPL/FEF and the SMG module is now labeled SMG/insula to more appropriately describe the distributed regions contained therein. Graph methods are as described in Figure 5 and text.

(B) The AG and IPS modules each split into multiple separate submodules, four of which (AG/mPFC [red], pIPL/sFG [light yellow], LIPS/dIPFC [light blue], aIPL/aPFC [light green]) contained regions within LLPC showing retrieval success effects. Regions in the right IPS and right dIPFC (RIPS/dIPFC, purple), cerebellum (light brown), and superior occipital cortex (SOC, teal) were also found to be distinct from the other regions. Parameters dictating the placement of nodes in network space are the same as in (A).

(C) Modularity optimization assignments shown in LLPC. Lines drawn in LLPC delineate submodule assignments. Colors are same as in (A) and (B). (D) Modularity optimization shown on lateral and medial views of the cortex using Caret software. Cerebellum (light brown in B) not shown. Colors are same as in (A) and (B) (see also Figure S2).

and function of locations spanning the entire cortex. In addition, it provides a set of ROIs that can be used to interrogate local functional distinctions and global network properties. The discussion that follows outlines the importance of the integrated analysis approach, as well as potential roles for the four “retrieval success” submodules defined in the graph theoretic analyses. In addition, other distinctions are outlined between our submodules and similar regions and networks that have been described in previous studies.

### An Integrated fMRI and rs-fcMRI Approach

One of the themes in the work presented here is the correspondence between networks discovered from data collected while subjects lie in the scanner fixating a central crosshair (rs-fcMRI), and data collected while subjects are engaged in a cognitively demanding task. These types of data differ not only on the basis of task demands (or lack thereof), but also in the time scales they sample. rs-fcMRI analyses here reflect correlations in low-frequency fluctuations of the blood oxygen level-dependent (BOLD) response (0.009–0.08 Hz) over many minutes, whereas task-related fMRI analyses reflect transient activations or deactivations over several seconds.

Why would such a high degree of similarity exist in networks defined from these seemingly disparate forms of data and analyses? We have hypothesized (Dosenbach et al., 2008; Fair et al., 2007) the answer to be rooted in a Hebbian-like mechanism whereby regions that tend to coactivate across task settings reduce the overall threshold for propagation of signals between

them via direct or indirect connections. Over time, the correlation between the “spontaneous” activity in two regions will tend to reflect their statistical history of coactivation across the myriad everyday “tasks” performed by the individual.

The approach employed here provides a means of identifying regions whose relationship can be gleaned from rs-fcMRI data and interrogated further in a variety of task settings, the combination of which has the potential to yield a richer set of results than can be obtained by each method individually.

### Regions in the LIPS/dIPFC Submodule Have Been Implicated in Processes Related to Familiarity Judgments and Attentional Control

In the context of memory retrieval studies, regions in left IPS have been implicated in a number of processing roles including, most notably, familiarity judgments (Henson et al., 1999; Wheeler and Buckner, 2004; Yonelinas et al., 2005). Recent metaanalytic studies have revealed the presence of consistent familiarity-related activation along the lateral bank of the IPS (Cabeza et al., 2008; Vilberg and Rugg, 2008), at or near the location of the regions described in our experiments (see Figure 7C). In addition, other experiments have shown familiarity-related activation in left dIPFC and dorsal frontal cortex (Yonelinas et al., 2005).

Studies not explicitly testing memory retrieval have also noted activity in similar regions. For instance, a metaanalysis published by Dosenbach et al. (2006) highlighted the presence of consistent start-cue effects in left IPS. This effect, which occurs when subjects are alerted that trials within a task block are about

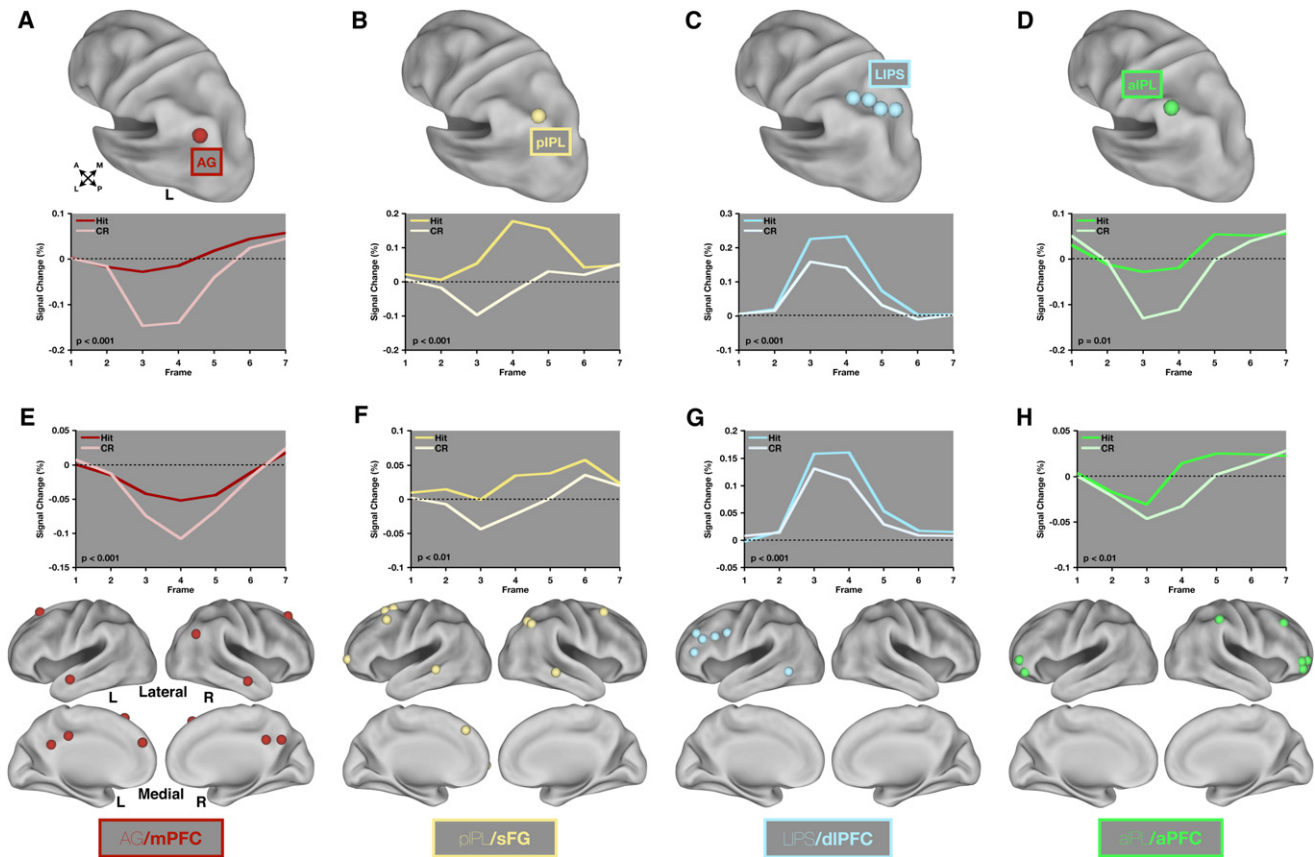


**Figure 7. Four rs-fcMRI-Derived Submodules Show Different Task-Evoked fMRI Time Course Dynamics and Retain Retrieval Success Effects Independent of the LLPC ROIs**

(A) A region in angular gyrus (AG) is shown on a lateral view of the left hemisphere using Caret software. Time courses (below) were extracted for hits and correct rejections across the eight studies that comprised the metaanalysis. *p* values represent the significance of the difference between hits and correct rejections determined by a response  $\times$  time repeated-measures ANOVA with two levels of response and seven levels of time.

(B–D) Same as in (A) but for piPL (B), LIPS (C), and aPLC (D).

(E) All ROIs in the AG/mPFC submodule excluding AG are shown on lateral and medial views of the cortex using Caret software. Time course data was extracted as in (A) but is averaged across all ROIs shown here. *p* values are same as in (A).

(F–H) Same as in (E) but for piPL/sFG (F), LIPS/dIPFC (G), and aPLC/aPFC (H).

to begin, appears to be domain general and is also seen when subjects are cued in a trial-wise manner to switch tasks or response contingencies (Bunge et al., 2002; Rushworth et al., 2001). Reliable start-cue effects are also seen in regions at or near bilateral dIPFC and dorsal frontal cortex.

Furthermore, this same set of regions appears to show greater responses when subjects make an error than when they respond correctly to a given item (Dosenbach et al., 2006; Wheeler et al., 2008). This effect, as with start cues, seems to occur largely independently of domain or task parameters. In addition to the task-evoked data, there is also evidence from functional connectivity data that regions in left IPS and dIPFC are part of a network (Dosenbach et al., 2007; Seeley et al., 2007) that supports flexible attentional control mechanisms.

Thus, activation of these regions during familiarity judgments may reflect control processes that are deployed when subjects are unable to determine with certainty whether an item is one they remember having encoded or not. In addition, reaction times for familiarity decisions tend to be greater than

“remember” or “new” judgments (Wheeler and Buckner, 2004; Yonelinas et al., 2005), perhaps reflecting additional demand on attentional resources.

It is important to note that the attention-related effects described here may be distinct from shifts in visuospatial attention and orienting that are characteristic of regions in the dorsal attention system (Corbetta and Shulman, 2002), which we believe are captured in the SPL/FEF submodule. Hutchinson et al. (2009) provide evidence along these lines using metaanalytic data to distinguish between regions at or near the LIPS/dIPFC submodule that show memory retrieval related effects and regions in the SPL that show consistent effects related to spatial attention in tasks not involving memory retrieval.

#### Regions in the AG/mPFC Submodule May Play a Role in Reinstating Context-Specific Perceptual Information

The AG/mPFC submodule consists of a number of regions that have been previously defined by task-induced deactivations

**Table 5. Post-Hoc Statistical Effects from the Submodule  $\times$  Time Repeated-Measures ANOVA and Response  $\times$  Time Repeated-Measures ANOVA within Each Submodule**

Submodules (w/o LLPC)	Submodule $\times$ Time
AG/mPFC versus pIPL/sFG	$F_{(6,108)} = 6.75, p < 0.001$
AG/mPFC versus aIPL/aPFC	$F_{(6,90)} = 6.21, p < 0.001$
AG/mPFC versus LIPS/dIPFC	$F_{(6,84)} = 47.06, p < 0.001$
pIPL/sFG versus aIPL/aPFC	$F_{(6,90)} = 0.38, p = 0.89$
pIPL/sFG versus LIPS/dIPFC	$F_{(6,84)} = 15.62, p < 0.001$
aIPL/aPFC versus LIPS/dIPFC	$F_{(6,66)} = 15.40, p < 0.001$
Submodule (w/o LLPC)	Response $\times$ Time
AG/mPFC	$F_{(6,54)} = 12.50, p < 0.001$
pIPL/sFG	$F_{(6,54)} = 3.41, p < 0.01$
aIPL/aPFC	$F_{(6,36)} = 4.85, p < 0.01$
LIPS/dIPFC	$F_{(6,90)} = 26.36, p < 0.001$

(Shulman et al., 1997). More recently, rs-fcMRI analyses have isolated a similar set of regions as being strongly correlated with one another when a subject is not in any specific task setting (Fox et al., 2005; Greicius et al., 2003). These regions have been termed the “default mode network” and encompass those obtained in the current study.

From the standpoint of memory retrieval, many of these regions have been implicated in a wide variety of processing roles including retrieval of autobiographical events or imagined future events (Schacter et al., 2007; Szpunar et al., 2007), remember judgments in the context of tasks probing recollection/familiarity distinctions (Henson et al., 1999; Wheeler and Buckner, 2004), and high-confidence recognition memory judgments (Yonelinas et al., 2005). In addition, a study from Kelley et al. (2002) has also highlighted a role for posterior cingulate and mPFC in making judgments related to trait adjectives that are self relevant. These regions, similar to those highlighted in autobiographical retrieval studies (McDermott et al., 2009), seem to be important when stimulus information is related more specifically to one’s own past. Similarly, the presence of activation in angular gyrus and other “default” regions for remember judgments may reflect the recollection of specific details from the encoding event, eliciting a greater sense that this item is “from their past.” Thus, the mechanism by which these regions support retrieval-related processing may be related to information that is not just simply “old,” but has a more specific autobiographical signature.

Support for the importance of “my” past in understanding activation in these regions comes from a study by Szpunar et al. (2009), in which subjects were asked to either remember events from their past or imagine personal events in the future; critically, some of these future events were to be set in places well known to the person, whereas others were to be set in unfamiliar settings. Activation in regions near angular gyrus and posterior cingulate was similar for conditions in which subjects remembered or imagined episodes in known contextual settings (e.g., one’s backyard), but was attenuated when the future event was projected to take place in a novel context (e.g., a safari). In short, activation in these regions was modulated not by whether a person was remembering an event or envisioning

a novel event, but was instead modulated by whether the event was placed in a well-known contextual setting or a novel setting.

### Regions in the aIPL/aPFC Submodule Are Consistent with Those Implicated in Postretrieval Monitoring

Regions in left lateral aPFC have been shown to support the retrieval of source information (Dobbins et al., 2002) and controlled semantic retrieval (Bunge et al., 2005) during memory-based tasks, but appear to show little or less activation during simple item memory judgments (Ranganath et al., 2000). Additionally, regions in right lateral aPFC have been most commonly attributed to source or post-retrieval monitoring (Dobbins et al., 2004). The claim that this signal occurs post retrieval relies on the fact that information related to the temporal signature of this activity in aPFC can be extracted. While the nature of the hemodynamic response can make it difficult to determine much in the way of timing relationships, late onset of activity has been noted in these regions both in fMRI (Henson et al., 2000; Reynolds et al., 2006; Schacter et al., 1997) and during ERP studies (Rugg and Allan, 2000).

An examination of the literature on aPFC will often show that IPL is activated for the same contrast (Dobbins et al., 2003, 2004), even though IPL regions are not typically highlighted. Regarding the late onset of the response, a recent study by Phillips et al. (2009) shows the time course of activity for a region very near our left aIPL region (see Figure 7D) that exhibits an early onset deactivation and a positive-going response that appears to take place much later than in regions showing a more canonical pattern of activity. This pattern of activation is similar to the time courses observed in a study by Reynolds et al. (2006) that also showed early onset deactivation with a very late positive onset, which was noted to likely be occurring post response.

Our metaanalytic time course data are consistent with similar types of processing that may occur post retrieval or post decision. Our data also appear to show an early onset deactivation of the time course relative to baseline that looks similar to the initial phase of the response in regions in the AG/mPFC submodule. This finding may be evidence that the activity in this region cannot be easily explained by a singular processing account. Further studies will need to be done in an attempt to tease out the implications of these timing dissociations to better understand their meaning in the context of memory retrieval and other task settings.

### The pIPL/sFG Submodule May Implement Processes Similar to Those in the aIPL/aPFC Submodule

The submodule analyses revealed a distinction between the pIPL/sFG submodule and the AG/mPFC submodule. There is little precedent in the literature for discussing processing distinctions in regions that may be interposed between AG and IPS, since typical regions of interest encompass much of one or the other. Based on the initial modularity optimization analysis (see Figure 5), the AG/mPFC and pIPL/sFG submodules appear closely linked as they comprised only one module. Interestingly, however, the time courses derived from the task-evoked fMRI data in AG/mPFC appear to be most similar to those in the aIPL/aPFC submodule (Figure 7; Table 3), with a negative response on CRs and little change from baseline on hits. One

possibility is that the pIPL/sFG submodule engages in similar post-decision processing mechanisms as the aIPL/aPFC submodule by virtue of its similar time course profile, but preferentially communicates with regions in the AG/mPFC submodule, as indicated by the rs-fcMRI analyses, to relay information related to the outcome of a trial.

### Three Distinctions Exist within a Previously Defined Unitary Fronto-Parietal Network

A study from Vincent et al. (2008) used rs-fcMRI to identify a network anatomically located between regions in the superior parietal lobule and the angular gyrus. In the current study, we find further separation of this network, which they termed the fronto-parietal control system (FPCS). Anatomically, the regions in LLPC that correspond to left IPS (LIPS/dIPFC submodule), aIPL (aIPL/aPFC submodule), and pIPL (pIPL/sFG submodule) all lie within the FPCS boundaries. Important additional evidence comes from the separation that we observe in bilateral frontal cortex. The extent of cortex corresponding to the FPCS in Vincent et al. (2008) contains regions that, in our hands, separate into the same distinctions we see in LLPC including the presence of separable members in dorsal frontal cortex and dIPFC (LIPS/dIPFC submodule), aPFC (aIPL/aPFC submodule), and superior frontal gyrus (pIPL/sFG submodule).

### Conclusion

Taken together, we found evidence that LLPC contains regions that are members of six submodules that span the cortex. This set of observations underscores the importance of interpreting data at a number of levels and with a number of different techniques. We think that this work reveals key organizational features of LLPC at both the region (local) and network (global) level that should inform future attempts to map function to structure.

## EXPERIMENTAL PROCEDURES

### Left Lateral Parietal Cortex: rs-fcMRI

#### Subjects

Subjects were recruited from the Washington University community and were screened with a self-report questionnaire to ensure that they had no current or previous history of neurological or psychiatric diagnosis. Informed consent was obtained from all subjects, and the study was approved by the Washington University Human Studies Committee. rs-fcMRI data were collected on 28 subjects (14 female, age 21–29 years) who were instructed to relax while fixating on a white cross on a black background. Three runs (2.5 s TR, 133 frames per run) were acquired on 21 subjects and two runs on the remaining seven subjects.

#### Data Acquisition

Images were acquired in adherence to a standard protocol. To help stabilize head position, each subject was fitted with a thermoplastic mask fastened to the head coil. All images were obtained with a Siemens MAGNETOM Tim Trio 3.0T scanner (Erlangen, Germany) and a Siemens 12 channel Head Matrix Coil. A T1-weighted sagittal MPRAGE structural image was obtained (TE = 3.08 ms, TR [partition] = 2.4 s, T1 = 1000 ms, flip angle = 8°, 176 slices with 1 × 1 × 1 mm voxels (Mugler and Brookeman, 1990). A T2-weighted turbo spin echo structural image (TE = 84 ms, TR = 6.8 s, 32 slices with 2 × 1 × 4 mm voxels) in the same anatomical plane as the BOLD images was also obtained to improve alignment to an atlas. An autoalign pulse sequence protocol provided in the Siemens software was used to align the acquisition

slices of the functional scans parallel to the anterior commissure-posterior commissure (AC-PC) plane and centered on the brain. This plane is parallel to the slices in the Talairach atlas (Talairach and Tournoux, 1988) which is used for subsequent data analysis. Functional imaging was performed using a BOLD contrast-sensitive gradient echo echo-planar sequence (TE = 27 ms, flip angle = 90°, in-plane resolution = 4 × 4 mm). Whole-brain EPI volumes (MR frames) of 32 contiguous, 4 mm-thick axial slices are obtained every 2.5 s. The first four image acquisitions were discarded to allow net magnetization to reach steady state.

#### MR Data Preprocessing

Imaging data from each subject were preprocessed to remove noise and artifacts, including: (1) correction for movement within and across runs using a rigid-body rotation and translation algorithm (Snyder, 1996), (2) whole-brain normalization to a common mode of 1000 to allow for comparisons across subjects (Ojemann et al., 1997), and (3) temporal realignment using sinc interpolation of all slices to the temporal midpoint of the first slice, accounting for differences in the acquisition time of each individual slice. Functional data were then resampled into 3 mm isotropic voxels and transformed into stereotaxic atlas space (Talairach and Tournoux, 1988). Atlas registration involved aligning each subject's T1-weighted image to a custom atlas-transformed (Lancaster et al., 1995) target T1-weighted template (711-2B) using a series of affine transforms (Michelon et al., 2003).

#### rs-fcMRI Preprocessing

Preprocessing for rs-fcMRI analyses was performed on the fMRI data as in Fox et al. (2005), to optimize the time-series data and remove spurious variance unlikely to reflect neuronal activity (e.g., heart rate and respiration). These steps included: (1) a temporal band-pass filter (0.009 Hz <  $f$  < 0.08 Hz) and spatial smoothing (6 mm full width at half maximum), (2) regression of six parameters obtained by rigid body head motion correction, (3) regression of the whole-brain signal (the average time course of the whole brain), (4) regression of ventricular signal extracted from ventricular ROIs, and (5) regression of white-matter signal extracted from white-matter ROIs. The first-order derivative terms for the movement, whole-brain, ventricular, and white-matter signals were also included in the correlation preprocessing.

#### Surface-Based Analysis

In Cohen et al. (2008), seeds were defined directly on the individual subject's flattened cortical representation. Here, the PALS atlas family of surfaces was used as a starting point to obtain common surface coordinates to use across our group of subjects (Van Essen, 2005). The PALS atlas "fiducial" surface represents the average of 12 individual gray midthickness surfaces each volumetrically registered to the 711-2B atlas. While the PALS fiducial surface does not represent the actual fiducial surface of any specific individual, it can be used to approximate average fiducial surface locations in group-averaged data in the same volumetric atlas space. Using Caret 5.3 software (Van Essen et al., 2001), a grid of seed points was generated on the spherical PALS surface over LLPC and the volumetric locations on the corresponding PALS fiducial surface in 711-2B atlas space were obtained.

#### rs-fcMRI Boundary Mapping

rs-fcMRI boundary mapping was then performed as in Cohen et al. (2008). For our purposes, the set of volumetric coordinates for a patch over LLPC was used to generate a set of 729 spherical ROIs (6 mm diameter). For each seed, in each subject, volumetric correlation maps were generated as in Fox et al. (2005), i.e., correlating the time course of a region of interest with the time courses of all other voxels over the entire volume of the brain. This method creates a volumetric correlation map for each seed. To generate maps of statistical significance, correlation maps were normalized using the Fisher  $r$ -to- $z$ -transform, and then converted into statistical  $z$ -scores. A volumetric average correlation map was then created for the group of subjects for each seed region, producing a single set of correlation maps representing the whole group, which is then used for the remaining analysis.

Eta<sup>2</sup> coefficients were calculated for all possible pairs of volumetric correlation maps, generating a 729 × 729 eta<sup>2</sup> matrix where each column represents the similarities between a particular region's volumetric correlation map and all

other regions' volumetric correlation maps. The full  $729 \times 729$   $\eta^2$  matrix was then reorganized into a series of 729 2D "patch-shaped" matrices such that each matrix represents the spatial organization of similarity between all the other seeds' correlation maps to the current seed's correlation map.

### Edge-Detection Algorithms

Since the matrix of  $\eta^2$  coefficients (i.e.,  $\eta^2$  profile) is a 2D array of values across the cortical surface, it can also be treated as a flat image. To find salient boundaries in these arrays, the Canny edge-detection algorithm (Canny, 1986), as implemented in the Image Processing Toolbox (v7.2) of the MATLAB software suite, was applied to each seed's  $\eta^2$  profile "image."

The Canny method smoothes the image with a Gaussian filter to reduce noise, and then creates a gradient image that locates regions that retain high spatial derivatives. High gradient values represent locations where the similarity between rs-fcMRI correlation maps is rapidly changing (i.e., they are peaks in the first derivative). After eliminating pixels in the 2D array that are not local maxima in the gradient image, the algorithm tracks along the highlighted regions of the image and categorizes each location as a boundary or not. To prevent hysteresis, both a high and low threshold are used. If the gradient magnitude of the pixel is below the low threshold, it is set to zero. If the magnitude is above the high threshold, it is considered a boundary. If the magnitude of the pixel is between the two thresholds, then the location is only considered a boundary if a neighboring pixel has a gradient above the high threshold. The primary goal is to identify and differentiate locations with strong, spatially coherent peaks as being different from locations that are relatively smooth or have incoherent gradient peaks across many of the  $\eta^2$  profiles. The result of processing the  $\eta^2$  profile set with an edge-detection algorithm is a set of binary images representing the locations of rapid changes in each grid point's  $\eta^2$  profile.

Since the boundary determination is binary, averaging across the entire set of binary edge maps generates a probabilistic boundary location map in which intensity represents how likely a location is to be a putative functional boundary.

### LLPC ROI Identification

Inverting the boundary location map provides a map of centroid locations, which can be used to generate regions using 2D local extrema algorithms (MATLAB v7.2, Image Processing Toolbox) as well as custom-written software that approximates established methods for detecting volumetric peaks of activation in task-evoked fMRI studies. The corresponding volumetric coordinates for each region identified are then used to generate spherical ROIs (10 mm diameter) for further analyses as described below.

### Left Lateral Parietal Cortex and Parietal-Cortical Networks: fMRI fMRI Metaanalysis of Studies Contrasting Hits versus Correct Rejections

Studies included a total of 140 neurologically normal adults between the ages of 18 to 35 who were recruited from both the Washington University and University of Pittsburgh communities. Data were collected on either a 1.5T Siemens MAGNETOM Vision Scanner (Washington University in St. Louis) or a 3T Siemens Allegra Scanner (University of Pittsburgh). Studies included a variety of different tasks in which judgments about item status were embedded within various source attribution, remember/know, or basic old/new decisions (Donaldson et al., 2010; Phillips et al., 2009; Velanova et al., 2003; Wheeler and Buckner, 2003, 2004) (Table 1). In addition, the encoding tasks contained either visual or auditory stimuli that were either presented once or many times to enhance retrieval success.

### MR Data Preprocessing

The same MR data preprocessing steps as used for the rs-fcMRI data (see above) were used for the fMRI data.

### Functional MRI Data Analysis Using the General Linear Model

BOLD activity related to the trials was modeled using a general linear model (GLM) approach. Additionally, baseline and trend terms for each BOLD run were included in the GLM. In each study, correct responses to both old and new items were coded separately, as were other manipulations that were

specific to each experiment. This approach is equivalent to estimating the finite impulse response evoked by each event and eschews assumptions about the form of the hemodynamic response function (Miezin et al., 2000; Ollinger et al., 2001; Zarahn et al., 1997).

### Analysis of Time Courses

rs-fcMRI derived regions were applied to the functional data to identify those that showed reliable retrieval success activity. Spherical ROIs with a diameter of 10 mm were created from the "peak" foci and the mean time course from all eight tasks for each of the regions was obtained for both hits and correct rejections.

### Parietal-Cortical Networks: rs-fcMRI rs-fcMRI "Neighborhood" Generation

As a means of determining the way in which LLPC regions differ from one another, the rs-fcMRI "neighborhoods," or the sets of regions that most strongly correlated with each identified region, were generated (see Figure 4B). A peak-finding algorithm was employed to determine the 15 most significant peaks of positive correlation for each LLPC ROI. The number of "neighbors" (15) represents an attempt to strike a balance between defining too few and too many neighbors for a given ROI. Too few neighbors would fail to adequately characterize a network corresponding to a given seed and too many neighbors would lead to the analysis of neighbors that are weakly correlated. As a result of this criterion, the lowest z-score of the Fisher  $r$ -to- $z$  transformed values that corresponded to the most minimally significant peak was not necessarily the same for each region. Nonetheless, all regions within each of the neighborhoods showed strongly significant effects ( $z\text{-score}_{\min} = 5.31$ ). In order to exclude regions with a significant degree of overlap, regions closer together than 10 mm were replaced by the average of their stereotactic coordinates.

### Modularity Optimization Analysis

Networks with  $N$  nodes (regions) can be mathematically represented as a  $N \times N$  matrix of relationships where cell  $ij$  contains the correlation coefficient of region  $i$  with region  $j$ . Our networks are formed from correlation matrices, which possess values from  $-1$  to  $1$ . These matrices may be thresholded, where cells below some value are set to zero. As thresholds rise, the density of edges in the network decreases, and at some point the network begins to fragment into disconnected components. The properties of graphs may change as edges are dropped from the network, and so it is important to explore a range of thresholds to determine whether network properties are dependent upon the threshold(s) being examined. An upper bound to this range is usually set by fragmentation considerations, and the lower bound is set to avoid negative and insignificant correlations.

Here, we report analyses from a (positive) range of thresholds over which significant modular structure was found ( $Q > 0.30$ ), and over which most nodes (>80%) could reach most other nodes, indicating that the network was minimally fragmented. Our module detection was performed with algorithms that optimize "modularity" (Fair et al., 2009; Newman, 2006; Newman and Girvan, 2004), a metric of modular structure in networks. Modularity ( $Q$ ) measures, for a given partition of a network into modules, the number of connections found within modules compared to the number of connections within modules expected by chance given the number of nodes and connections in the network. Our algorithm maximizes this metric, and returns the node assignments into modules that yield the highest value. Typically,  $Q$  values over 0.30 are thought to indicate strong community structure (Fortunato, 2010; Newman, 2006).

### Spring Embedding Using Social Network Image Animator

Though the correlation matrix contains a complete description of the network, it is information dense and difficult to inspect visually. To visualize the network structure, we used a standard technique called spring embedding. Graphs were created by using the Kamada-Kawai spring-embedding algorithm implemented in the Social Network Image Animator (SoNIA) software package (Bender-deMoll and McFarland, 2006).

Nodes were given a fixed-repulsive force and placed randomly in a plane, and springs with force constants related to the pairwise correlation coefficients

of the matrix were placed between all nodes. This spring system was allowed to iteratively reposition nodes in order to reduce the energy of the spring system, resulting in a final low-energy state, where nodes with high correlations are positioned near one another, and those with weak or no connections are placed more distantly.

Spring-embedding diagrams were combined with module assignments to reveal individual node-node interactions, and the relationships of modules to one another.

#### SUPPLEMENTAL INFORMATION

Supplemental Information includes two figures (modularity optimization assignments from Figures 5 and 6 across a broad range of correlation thresholds as well as plots of modularity optimization parameters) and can be found with this article online at doi:10.1016/j.neuron.2010.05.025.

#### ACKNOWLEDGMENTS

We thank Kathleen McDermott, Kelly Barnes, Nico Dosenbach, Jessica Church, Alecia Vogel, Christopher Fetsch, and Maital Neta for helpful discussion; Mark McAvoy and Avi Snyder for technical support; and Randy Buckner for generously providing data. Funding for this work came from National Institutes of Health grants NS32979 (S.E.P.), NS41255 (S.E.P.), NS46424 (S.E.P.), NS62489 (A.L.C.), and NS53425 (B.L.S.).

Accepted: May 19, 2010

Published: July 14, 2010

#### REFERENCES

- Bender-deMoll, S., and McFarland, D.A. (2006). The art and science of dynamic network visualization. *J. Soc. Struct.* 7, 2.
- Biswal, B., Yetkin, F., Haughton, V., and Hyde, J. (1995). Functional connectivity in the motor cortex of resting human brain using echo-planar MRI. *Magn. Reson. Med.* 34, 537–541.
- Bullmore, E., and Sporns, O. (2009). Complex brain networks: graph theoretical analysis of structural and functional systems. *Nat. Rev. Neurosci.* 10, 186–198.
- Bunge, S.A., Hazeltine, E., Scanlon, M.D., Rosen, A.C., and Gabrieli, J.D. (2002). Dissociable contributions of prefrontal and parietal cortices to response selection. *Neuroimage* 17, 1562–1571.
- Bunge, S.A., Wendelken, C., Badre, D., and Wagner, A.D. (2005). Analogical reasoning and prefrontal cortex: evidence for separable retrieval and integration mechanisms. *Cereb. Cortex* 15, 239–249.
- Cabeza, R., Ciaramelli, E., Olson, I.R., and Moscovitch, M. (2008). The parietal cortex and episodic memory: an attentional account. *Nat. Rev. Neurosci.* 9, 613–625.
- Canny, J. (1986). A computational approach to edge detection. *IEEE Trans. Pattern Anal. Mach. Intell. PAMI-8*, 679–698.
- Ciaramelli, E., Grady, C., and Moscovitch, M. (2008). Top-down and bottom-up attention to memory: A hypothesis (AtoM) on the role of the posterior parietal cortex in memory retrieval. *Neuropsychologia* 46, 1828–1851.
- Cohen, A.L., Fair, D.A., Dosenbach, N.U., Miezin, F.M., Dierker, D., Van Essen, D.C., Schlaggar, B.L., and Petersen, S.E. (2008). Defining functional areas in individual human brains using resting functional connectivity MRI. *Neuroimage* 41, 45–57.
- Corbetta, M., and Shulman, G. (2002). Control of goal-directed and stimulus-driven attention in the brain. *Nat. Rev. Neurosci.* 3, 201–215.
- Corbetta, M., Akbudak, E., Conturo, T.E., Snyder, A.Z., Ollinger, J.M., Drury, H.A., Linenweber, M.R., Petersen, S.E., Raichle, M.E., Van Essen, D.C., and Shulman, G.L. (1998). A common network of functional areas for attention and eye movements. *Neuron* 21, 761–773.
- Devlin, J.T., and Poldrack, R.A. (2007). In praise of tedious anatomy. *Neuroimage* 37, 1033–1041.
- Dobbins, I.G., Foley, H., Schacter, D.L., and Wagner, A.D. (2002). Executive control during episodic retrieval: multiple prefrontal processes subservice source memory. *Neuron* 35, 989–996.
- Dobbins, I.G., Rice, H.J., Wagner, A.D., and Schacter, D.L. (2003). Memory orientation and success: separable neurocognitive components underlying episodic recognition. *Neuropsychologia* 41, 318–333.
- Dobbins, I.G., Simons, J.S., and Schacter, D.L. (2004). fMRI evidence for separable and lateralized prefrontal memory monitoring processes. *J. Cogn. Neurosci.* 16, 908–920.
- Donaldson, D.I., Wheeler, M.E., and Petersen, S.E. (2010). Remember the source: dissociating frontal and parietal contributions to episodic memory. *J. Cogn. Neurosci.* 22, 377–391.
- Dosenbach, N.U.F., Visscher, K.M., Palmer, E.D., Miezin, F.M., Wenger, K.K., Kang, H.C., Burgund, E.D., Grimes, A.L., Schlaggar, B.L., and Petersen, S.E. (2006). A core system for the implementation of task sets. *Neuron* 50, 799–812.
- Dosenbach, N.U.F., Fair, D.A., Miezin, F.M., Cohen, A.L., Wenger, K.K., Dosenbach, R.A.T., Fox, M.D., Snyder, A.Z., Vincent, J.L., Raichle, M.E., et al. (2007). Distinct brain networks for adaptive and stable task control in humans. *Proc. Natl. Acad. Sci. USA* 104, 11073–11078.
- Dosenbach, N.U.F., Fair, D.A., Cohen, A.L., Schlaggar, B.L., and Petersen, S.E. (2008). A dual-networks architecture of top-down control. *Trends Cogn. Sci.* 12, 99–105.
- Fair, D.A., Dosenbach, N.U.F., Church, J.A., Cohen, A.L., Brahmbhatt, S., Miezin, F.M., Barch, D.M., Raichle, M.E., Petersen, S.E., and Schlaggar, B.L. (2007). Development of distinct control networks through segregation and integration. *Proc. Natl. Acad. Sci. USA* 104, 13507–13512.
- Fair, D.A., Cohen, A.L., Power, J.D., Dosenbach, N.U.F., Church, J.A., Miezin, F.M., Schlaggar, B.L., and Petersen, S.E. (2009). Functional brain networks develop from a “local to distributed” organization. *PLoS Comput. Biol.* 5, e1000381.
- Fortunato, S. (2010). Community detection in graphs. *Phys. Rep.* 486, 75–174.
- Fox, M.D., Snyder, A.Z., Vincent, J.L., Corbetta, M., Van Essen, D.C., and Raichle, M.E. (2005). The human brain is intrinsically organized into dynamic, anticorrelated functional networks. *Proc. Natl. Acad. Sci. USA* 102, 9673–9678.
- Göbel, S.M., and Rushworth, M.F. (2004). Cognitive neuroscience: acting on numbers. *Curr. Biol.* 14, R517–R519.
- Greicius, M.D., Krasnow, B., Reiss, A.L., and Menon, V. (2003). Functional connectivity in the resting brain: a network analysis of the default mode hypothesis. *Proc. Natl. Acad. Sci. USA* 100, 253–258.
- Henson, R.N., Rugg, M.D., Shallice, T., Josephs, O., and Dolan, R.J. (1999). Recollection and familiarity in recognition memory: an event-related functional magnetic resonance imaging study. *J. Neurosci.* 19, 3962–3972.
- Henson, R.N., Rugg, M.D., Shallice, T., and Dolan, R.J. (2000). Confidence in recognition memory for words: Dissociating right prefrontal roles in episodic retrieval. *J. Cogn. Neurosci.* 12, 913–923.
- Hubbard, E.M., Piazza, M., Pinel, P., and Dehaene, S. (2005). Interactions between number and space in parietal cortex. *Nat. Rev. Neurosci.* 6, 435–448.
- Hutchinson, J.B., Uncapher, M.R., and Wagner, A.D. (2009). Posterior parietal cortex and episodic retrieval: convergent and divergent effects of attention and memory. *Learn. Mem.* 16, 343–356.
- Kelley, W.M., Macrae, C.N., Wyland, C.L., Caglar, S., Inati, S., and Heatherton, T.F. (2002). Finding the self? An event-related fMRI study. *J. Cogn. Neurosci.* 14, 785–794.
- Konishi, S., Wheeler, M.E., Donaldson, D.I., and Buckner, R.L. (2000). Neural correlates of episodic retrieval success. *Neuroimage* 12, 276–286.
- Lancaster, J.L., Glass, T.G., Lankipalli, B.R., Downs, H., Mayberg, H., and Fox, P.T. (1995). A modality-independent approach to spatial normalization of tomographic images of the human brain. *Hum. Brain Mapp.* 3, 209–223.
- McDermott, K.B., Jones, T.C., Petersen, S.E., Lageman, S.K., and Roediger, H.L., III. (2000). Retrieval success is accompanied by enhanced activation in

- anterior prefrontal cortex during recognition memory: an event-related fMRI study. *J. Cogn. Neurosci.* 12, 965–976.
- McDermott, K.B., Szpunar, K.K., and Christ, S.E. (2009). Laboratory-based and autobiographical retrieval tasks differ substantially in their neural substrates. *Neuropsychologia* 47, 2290–2298.
- Michelon, P., Snyder, A.Z., Buckner, R.L., McAvoy, M., and Zacks, J.M. (2003). Neural correlates of incongruous visual information. An event-related fMRI study. *Neuroimage* 19, 1612–1626.
- Miezin, F.M., Maccotta, L., Ollinger, J.M., Petersen, S.E., and Buckner, R.L. (2000). Characterizing the hemodynamic response: Effects of presentation rate, sampling procedure, and the possibility of ordering brain activity based on relative timing. *Neuroimage* 11, 735–759.
- Mugler, J.P., III, and Brookeman, J.R. (1990). Three-dimensional magnetization-prepared rapid gradient-echo imaging (3D MP RAGE). *Magn. Reson. Med.* 15, 152–157.
- Newman, M.E. (2006). Modularity and community structure in networks. *Proc. Natl. Acad. Sci. USA* 103, 8577–8582.
- Newman, M.E.J., and Girvan, M. (2004). Finding and evaluating community structure in networks. *Phys. Rev. E Stat. Nonlin. Soft Matter Physiol.* 69, 026113.
- Ojemann, J.G., Akbudak, E., Snyder, A.Z., McKinstry, R.C., Raichle, M.E., and Conturo, T.E. (1997). Anatomic localization and quantitative analysis of gradient refocused echo-planar fMRI susceptibility artifacts. *Neuroimage* 6, 156–167.
- Ollinger, J.M., Shulman, G.L., and Corbetta, M. (2001). Separating processes within a trial in event-related functional MRI I. The method. *Neuroimage* 13, 210–217.
- Phillips, J.S., Velanova, K., Wolk, D.A., and Wheeler, M.E. (2009). Left posterior parietal cortex participates in both task preparation and episodic retrieval. *Neuroimage* 46, 1209–1221.
- Ranganath, C., Johnson, M.K., and D'Esposito, M. (2000). Left anterior prefrontal activation increases with demands to recall specific perceptual information. *J. Neurosci.* 20, 1–5.
- Reynolds, J.R., McDermott, K.B., and Braver, T.S. (2006). A direct comparison of anterior prefrontal cortex involvement in episodic retrieval and integration. *Cereb. Cortex* 16, 519–528.
- Rugg, M.D., and Allan, K. (2000). Event-related potential studies of memory. In *The Oxford Handbook of Memory*, E. Tulving and F.J.M. Craik, eds. (Oxford: Oxford University Press), pp. 521–537.
- Rushworth, M.F.S., Paus, T., and Sipila, P.K. (2001). Attention systems and the organization of the human parietal cortex. *J. Neurosci.* 21, 5262–5271.
- Schacter, D.L., Buckner, R.L., Koutstaal, W., Dale, A.M., and Rosen, B.R. (1997). Late onset of anterior prefrontal activity during true and false recognition: An event-related fMRI study. *Neuroimage* 6, 259–269.
- Schacter, D.L., Addis, D.R., and Buckner, R.L. (2007). Remembering the past to imagine the future: the prospective brain. *Nat. Rev. Neurosci.* 8, 657–661.
- Seeley, W.W., Menon, V., Schatzberg, A.F., Keller, J., Glover, G.H., Kenna, H., Reiss, A.L., and Greicius, M.D. (2007). Dissociable intrinsic connectivity networks for salience processing and executive control. *J. Neurosci.* 27, 2349–2356.
- Shulman, G.L., Fiez, J.A., Corbetta, M., Buckner, R.L., Miezin, F.M., Raichle, M.E., and Petersen, S.E. (1997). Common blood flow changes across visual tasks: II. Decreases in cerebral cortex. *J. Cogn. Neurosci.* 9, 648–663.
- Simons, J.S., Peers, P.V., Hwang, D.Y., Ally, B.A., Fletcher, P.C., and Budson, A.E. (2008). Is the parietal lobe necessary for recollection in humans? *Neuropsychologia* 46, 1185–1191.
- Snyder, A.Z. (1996). Difference image vs. ratio image error function forms in PET-PET realignment. In *Quantification of Brain Function Using PET*, R. Myer, V.J. Cunningham, D.L. Bailey, and T. Jones, eds. (San Diego, CA: Academic Press), pp. 131–137.
- Sporns, O., and Zwi, J.D. (2004). The small world of the cerebral cortex. *Neuroinformatics* 2, 145–162.
- Szpunar, K.K., Watson, J.M., and McDermott, K.B. (2007). Neural substrates of envisioning the future. *Proc. Natl. Acad. Sci. USA* 104, 642–647.
- Szpunar, K.K., Chan, J.C.K., and McDermott, K.B. (2009). Contextual processing in episodic future thought. *Cereb. Cortex* 19, 1539–1548.
- Talairach, J., and Tournoux, P. (1988). *Co-Planar Stereotaxic Atlas of the Human Brain* (New York: Thieme Medical Publishers, Inc.).
- Turkeltaub, P.E., Eden, G.F., Jones, K.M., and Zeffiro, T.A. (2002). Meta-analysis of the functional neuroanatomy of single-word reading: method and validation. *Neuroimage* 16, 765–780.
- Van Essen, D.C. (2005). A population-average, landmark- and surface-based (PALS) atlas of human cerebral cortex. *Neuroimage* 28, 635–662.
- Van Essen, D.C., Dickson, J., Harwell, J., Hanlon, D., Anderson, C.H., and Drury, H.A. (2001). An integrated software suite for surface-based analyses of cerebral cortex. *J. Am. Med. Inform. Assoc.* 8, 443–459.
- Velanova, K., Jacoby, L.L., Wheeler, M.E., McAvoy, M.P., Petersen, S.E., and Buckner, R.L. (2003). Functional-anatomic correlates of sustained and transient processing components engaged during controlled retrieval. *J. Neurosci.* 23, 8460–8470.
- Vilberg, K.L., and Rugg, M.D. (2008). Memory retrieval and the parietal cortex: a review of evidence from a dual-process perspective. *Neuropsychologia* 46, 1787–1799.
- Vincent, J.L., Kahn, I., Snyder, A.Z., Raichle, M.E., and Buckner, R.L. (2008). Evidence for a frontoparietal control system revealed by intrinsic functional connectivity. *J. Neurophysiol.* 100, 3328–3342.
- Wagner, A.D., Shannon, B.J., Kahn, I., and Buckner, R.L. (2005). Parietal lobe contributions to episodic memory retrieval. *Trends Cogn. Sci.* 9, 445–453.
- Wheeler, M.E., and Buckner, R.L. (2003). Functional dissociation among components of remembering: Control, perceived oldness, and content. *J. Neurosci.* 23, 3869–3880.
- Wheeler, M.E., and Buckner, R.L. (2004). Functional-anatomic correlates of remembering and knowing. *Neuroimage* 21, 1337–1349.
- Wheeler, M.E., Petersen, S.E., Nelson, S.M., Ploran, E.J., and Velanova, K. (2008). Dissociating early and late error signals in perceptual recognition. *J. Cogn. Neurosci.* 20, 2211–2225.
- Yantis, S., Schwarzbach, J., Serences, J.T., Carlson, R.L., Steinmetz, M.A., Pekar, J.J., and Courtney, S.M. (2002). Transient neural activity in human parietal cortex during spatial attention shifts. *Nat. Neurosci.* 5, 995–1002.
- Yonelinas, A.P., Otten, L., Shaw, K., and Rugg, M. (2005). Separating the brain regions involved in recollection and familiarity in recognition memory. *J. Neurosci.* 25, 3002–3008.
- Zarahn, E., Aguirre, G., and D'Esposito, M. (1997). A trial-based experimental design for fMRI. *Neuroimage* 6, 122–138.